**JMATPRO** 

# Journal of Advanced Materials and Processing 11 (44): 55-69, Autumn 2023 https://sanad.iau.ir/journal/jmatpro

Doi: 10.71670/jmatpro.2023.1204326

Research Paper

# Investigating the Microstructure and Mechanical Properties of Tantalum Sintered Parts by Hot Pressing in a Vacuum

# Farrokh Najafzadegan<sup>1</sup>, Alireza Khodabandeh<sup>1\*</sup>, Hossein Youzbashizadeh<sup>2</sup>, Morteza Tamizifar<sup>3</sup>

- 1. Department of Materials Science and Engineering, Science and Research Branch, Islamic Azad University, Tehran, Iran.
- 2. Department of Materials Science and Engineering, Sharif University of Technology, Tehran, Iran.
- 3. School of Metallurgy and Materials Engineering, Iran University of Science and Technology, Narmak, Tehran, Iran.

# **ARTICLE INFO**

Article history:

Received 18 April 2025 Revised: 11 June 2025 Accepted 15 September 2025 Available online 1 October 2023

Keywords: Tantalum Hot Pressing Ductility Mechanical Properties

# **ABSTRACT**

This study investigates the consolidation of pure tantalum powder via hot pressing (HP) to enhance its ductility and mechanical properties. The effects of sintering temperature and time on the microstructure and mechanical properties of sintered tantalum were examined. Density was measured using the Archimedes method, while microstructure was analyzed via optical and scanning electron microscopy. Compression tests evaluated mechanical properties. Results revealed that reduced porosity and altered porosity morphology significantly improved mechanical properties. A 17.6% density increase led to a 100% enhancement in compressive strength, ductility, and hardness. Optimal properties were achieved at 1600°C, yielding a hardness of 345 HV, compressive strength of 1278 MPa, and ductility of 34%.

**Citation**: Najafzadegan, F.; Khodabandeh, A.; Youzbashizadeh, H.; Tamizifar, M. (2023). Investigating the Microstructure and Mechanical Properties of Tantalum Sintered Parts by Hot Pressing in a Vacuum, Journal of Advanced Materials and Processing, 11 (44), 55-69. Doi: 10.71670/jmatpro.2023.1204326

#### Copyrights:

Copyright for this article is retained by the author (s), with publication rights granded to Journal of Advanced Materials and Processing. This is an open – acsses article distributed under the terms of the Creative Commons Attribution License (<a href="http://creativecommons.org/licenses/by/4.0">http://creativecommons.org/licenses/by/4.0</a>), which permits unrestricted use, distribution and reproduction in any medium, provided the original work is properly cited.



E-Mail: alireza.khodabandeh@etsmtl.ca

<sup>\*</sup> Corresponding Author:

#### 1. Introduction

Tantalum exhibits unique properties among refractory metals, including a high melting point, compatibility with interstitial elements, an appropriate elastic modulus, and excellent room-temperature formability, making it ideal for diverse applications [1]. Its high density and flexibility support its use in high strain-rate applications [2], and its formability makes it a preferred material in specific contexts [3, 4]. However, its high cost and application in military armaments have limited its widespread adoption [5, 6]. Recent studies have significantly advanced efforts to reduce costs and eliminate heterogeneous structures [7, 8].

Sintering tantalum powder is challenging due to its high melting point, low thermal conductivity, and strong affinity for interstitial elements, requiring high temperatures, extended sintering times, and vacuum conditions in powder metallurgy processes [9]. Using nano-powders enhances sinterability [10]. Hot pressing, which applies simultaneous pressure and heat, effectively produces high-density parts with controlled microstructures. Vacuum hot pressing with rapid induction heating is particularly suitable for sintering powders, especially nano-powders, minimizing the gap between theoretical and actual densities.

Mort et al. investigated oxygen and carbon dissolution and precipitation in tantalum powder after hot pressing, identifying various oxide and carbide precipitates using microscopy and XRD [11]. Stkra reported a hardness of 120 Vickers for 99.95% pure tantalum, which increased to 500 Vickers with 2.4% oxygen content [12]. Dragkamp et al. used machined tantalum powder, controlling oxygen contamination by limiting new surface formation [13]. Mann's work demonstrated that machining chip powder provides a framework for studying oxygen's role in tantalum's structural development [14]. Angerer et al. achieved a maximum relative density of 95% in hot-pressed tantalum at 1700°C for 60 minutes under 30 MPa pressure, with residual stress analyzed via X-ray diffraction [15, 16]. Despite these advances, the effects of sintering parameters on tantalum's microstructure and mechanical properties during hot pressing remain underexplored.

This study investigates how hot pressing parameters, such as sintering temperature and time, affect tantalum's sintering behavior and microstructure. The relationship between porosity morphology and mechanical properties is examined to identify optimal sintering conditions for achieving superior mechanical performance.

#### 2. Materials and Methods

In this study, tantalum powder from Aldrich Company was used. Table 1 shows the chemical composition of the purchased tantalum powder.

 Trace Metal Analysis
 =< 1000 ppm</td>

 Chromium (Cr)
 14.0 ppm

 Iron (Fe)
 23.0 ppm

 Molybdenum (Mo)
 190.0 ppm

 Nickel (Ni)
 16.0 ppm

 Tungsten (W)
 280.0 ppm

**Table 1.** Chemical Composition of Tantalum Powder.

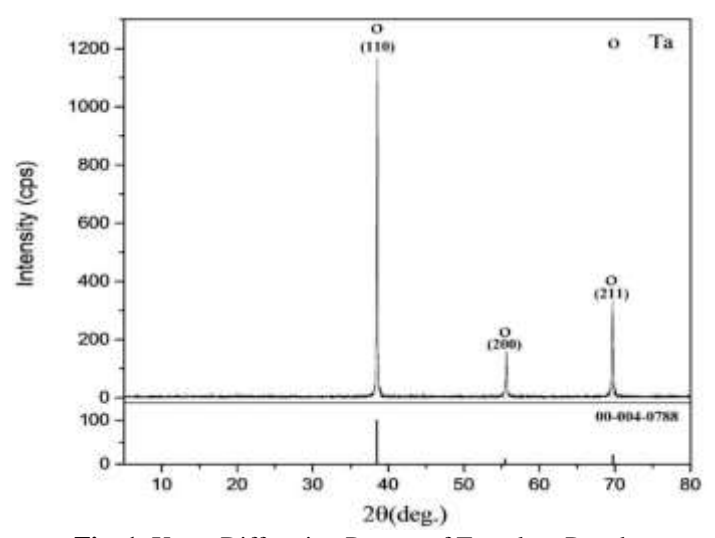


Fig. 1. X-ray Diffraction Pattern of Tantalum Powder

A Philips X-PERT X-ray diffractometer was used to examine the purchased powder. Fig. 1 shows the X-ray diffraction pattern of the tantalum powder, which shows only the tantalum phase.

Fig. 2 shows the scanning electron microscope image of the tantalum powder. The powder morphology was

irregular and without any significant agglomeration. The particle size of the powder was determined by scanning electron microscopy by measuring more than 30 particles, and the average particle size was reported to be 1.44 microns.

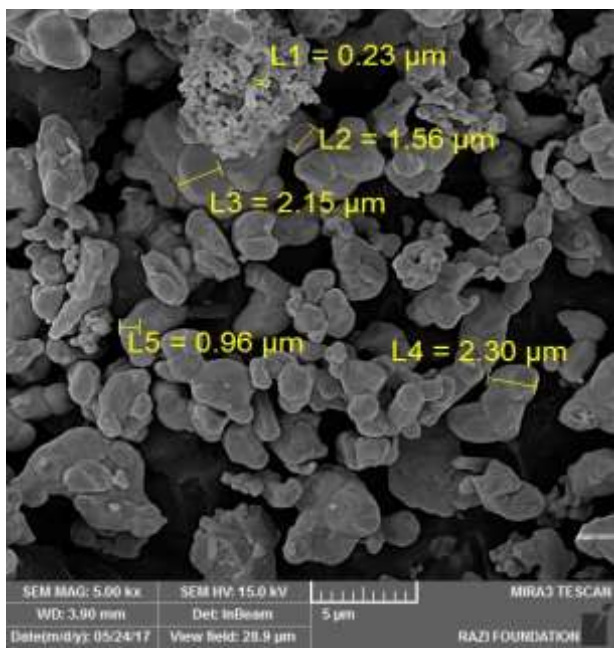


Fig. 2. Scanning Electron Microscope Image of Tantalum Powder.

A graphite mold was used to fabricate the samples. Graphite foil was used on the inner surfaces of the mold to prevent mold wear and chemical reaction with the tantalum powder. Solidification was carried out using a vacuum hot press with a hydraulic system and a capacity of 15 tons. The mold and powder

assembly were placed between two punches inside the hot press chamber. The dimensions of the graphite mold used are schematically shown in Fig. 3. Density was measured by the Archimedes method in water according to ASTM B 527 standard requirements.

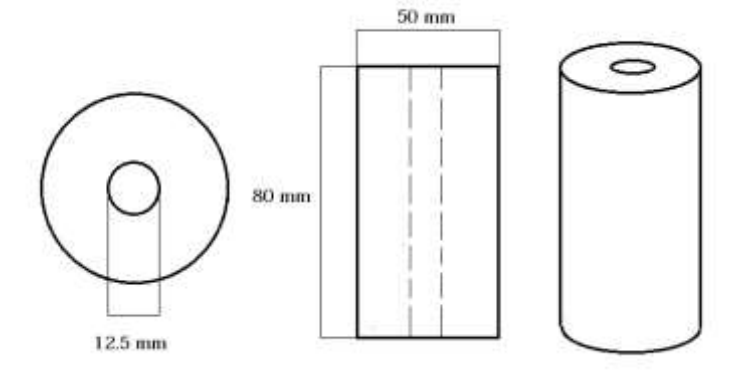


Fig. 3. Dimensions of Graphite Mold

Table 2 details the vacuum hot pressing conditions, and Table 3 shows Specimen conditions.

Table 2	Details of	Vacuum	Hot 1	Pressing	Conditions.
Table 2.	Details of	v acuum	HUL.	LICSSIIIE	Continuons.

Mold diameter	12.5 mm			
powder in each sample	12 gram			
pressure	40 MPa			
Heating rate	100 °C/min			
Vacuum	5*10 <sup>-2</sup> mbar			
thermocouple type	Type-R			

**Table 3.** Specimen conditions.

Temperature	Time				
°C	min				
1400	20				
1500	15				
1500	25				
1600	20				
	Temperature °C 1400 1500				

To examine the microstructure, initial preparation such as sanding and polishing was performed, and diamond paste was used in the final polishing of the samples. After the preparation operations on the samples, etching was performed for 30 seconds using an H<sub>2</sub>O:HNO<sub>3</sub>:HF: H<sub>2</sub>SO<sub>4</sub> solution with ratios of 1:1:1:3. Microstructure examination was performed by optical microscopy and scanning electron microscopy. The grain size was determined according to the planimetric method in ASTM E112 standard by measuring more than 90 grains from each sample and determining the average grain size. SIS image processing software was used to determine the size, distribution, and morphology of the Porosity. Hardness measurement on the samples after the hot pressing process was performed by a Buhler Vickers microhardness tester according to ASTM E384 standard requirements. Vickers microhardness measurement was performed with an average of 3 hardness impressions under a load of 9.807 N. To examine the mechanical properties of the samples, a compression test was performed at room temperature according to ASTM E9 standard requirements. In this test, samples with a ratio of h<sub>0</sub>/d<sub>0</sub>=1.1 (h<sub>0</sub> initial height and d<sub>0</sub> initial diameter of the sample) and a compression test with a loading rate of 1 mm/min were performed by an Instron-8503 device. To calculate the percentage of porosity in the samples, Equation (1) was used based on the density:

$$P = 1 - \left(\frac{\rho}{\rho_0}\right) \tag{1}$$

In this relation, P is the percentage of porosity,  $\rho$  is the density of the porous material, and  $\rho 0$  is the density of the material in a non-porous state (theoretical density). The equivalent diameter factor was used to examine the Porosity characteristics. The equivalent diameter factor, Dcircle, is equal to the

diameter of a circle that has an area equal to the metallographic cross-sectional area of the Porosity. In order to examine the equivalent diameter factor, Equation (2) was used:

$$D_{circle} = 2\sqrt{A}/\pi \tag{2}$$

The effective load-bearing cross-sectional area is considered as one of the variables of interest in sintered materials. The value of the effective cross-sectional area of load bearing was calculated using equation (3):

$$A_{t} = A_{0}(1-P) \tag{3}$$

In this relation,  $A_0$  is the apparent surface area, P is the total porosity percentage, and  $A_t$  is the effective load-bearing cross-sectional area [17].

# 3. Results and Discussion

The primary parameters influencing the solid-state sintering process are sintering temperature, sintering time, and powder particle size, which collectively determine the metallurgical properties of components produced through powder metallurgy. In solid-state sintering, densification occurs through deformation of powder particles, driven by atomic diffusion, porosity reduction, and grain growth. During this process, the solid-gas interface is replaced by a solid-solid interface, reducing the driving force for sintering. This method necessitates high temperatures and fine powder particles to enable atomic diffusion and achieve densification over an appropriate time period.

Smaller powder particle sizes increase the surface-to-volume ratio, thereby enhancing the sintering rate, particularly in the initial stage. During this stage, initial bonds form between powder particles, leading to neck growth. As sintering progresses, the neck area expands, and the centers of adjacent particles move

closer together. The driving force for atomic diffusion and movement toward the neck region or porosity is determined by the chemical potential gradient, influenced by vacancy concentration beneath the particle surface. Atoms migrate from regions of higher chemical potential to those of lower potential, activating mass transfer mechanisms.

Structural changes associated with neck growth during sintering are governed by diffusion processes. Generally, finer particles result in faster neck growth rates due to their higher surface-to-volume ratio. By optimizing sintering time and temperature, superior outcomes can be achieved [18]. In this study, the average particle size was reported as 1.44 microns. The use of finer powders, which increases the surface-to-volume ratio and sintering driving force, enables sintering at lower temperatures and shorter times, improving powder densification behavior.

Figure 4 illustrates the relative density of the samples. The green density of the samples was 60% of the theoretical density. At a sintering temperature of 1400°C, the relative density increased to 80% of the theoretical density. A near-theoretical density of 97.6% was achieved at 1600°C.

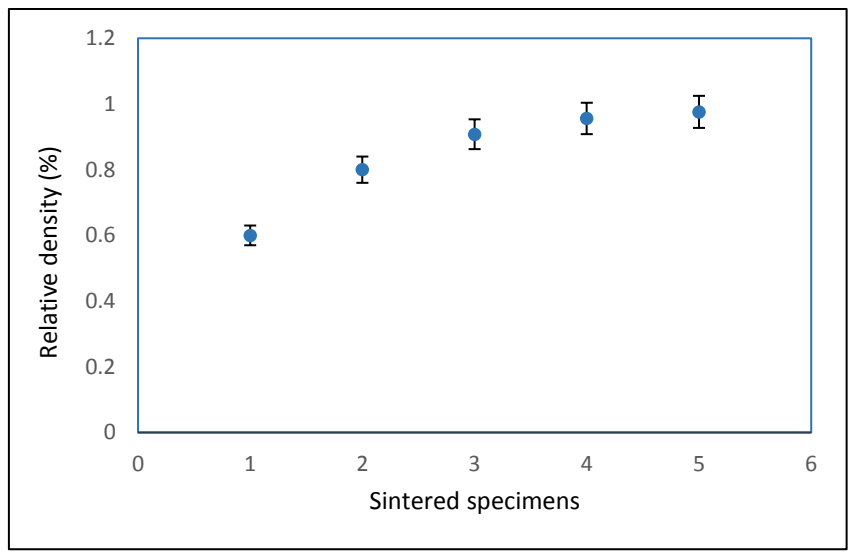


Fig. 4. Relative Density Diagram of Samples.

The results indicate that, as the temperature increases, the theoretical density rises by approximately 17.6%. This increase can be attributed to the enhanced diffusion process, which is thermally activated. Atomic movement depends on the energy required to jump into vacancies. The multiplicity of atomic vacancies, as well as the number of atoms with sufficient energy to migrate into these vacancies, can be determined using the Arrhenius equation Equation

$$\frac{N}{N_0} = e^{\left(\frac{-Q}{RT}\right)} \tag{4}$$

 $N/N_0$  is the ratio of available vacancies (activated atoms) to the total atoms, Q is the activation energy of tantalum (413.3 kJ/mol), R is the universal gas constant, and T is the temperature in Kelvin [19]. The N/N<sub>0</sub> ratio for tantalum at 1400°C and 1600°C was calculated to be  $6.48*10^{-14}$  and  $1.77*10^{-12}$ , respectively. The results showed that temperature has a significant effect on the vacancy ratio, and with increasing temperature, the ratio of vacancies to total atoms increased by 27%. On the other hand, the diffusion coefficient of tantalum was calculated according to Equation (5).

$$D_{\text{tantalum}} = 1.24^{*4} - 10 \ e^{\left(\frac{-Q}{RT}\right)}$$
 (5)

In this relation, D is the diffusion coefficient,  $D_0$  is the intrinsic diffusion coefficient of tantalum (1.24 \* 10<sup>-4</sup> m<sup>2</sup>/sec), Q is the activation energy of tantalum (413.3 kJ/mol), R is the universal gas constant, and T is the temperature in Kelvin [19].

The diffusion coefficient of tantalum at 1400°C and 1600°C was calculated to be 8.04 \* 10<sup>-18</sup> m<sup>2</sup>/sec and 2.19 \* 10<sup>-16</sup> m<sup>2</sup>/sec, respectively. The results showed that temperature has a very significant effect on the diffusion coefficient, and with an increase in temperature from 1400°C to 1600°C, the diffusion coefficient increased by 27 %. With increasing temperature, the number of active atoms and the necessary vacancies for movement increased. Increasing temperature increases the grain boundary excitability and reduces the porosity in the sample, ultimately leading to an increase in density.

At 1500°C, with increasing sintering time, the relative density increased from 90.86% to 95.65% of the theoretical density. The relative density of the samples increased by 5% with increasing sintering time. The sintering mechanism can be explained using Equations (6) and (7).

$$K = e^{(A - \frac{Q}{RT})} \tag{6}$$

$$K = e^{(A - \frac{Q}{RT})}$$

$$Lg \frac{\Delta L}{L_0} = n Lg t + Lg k$$
(6)
(7)

In this relation, K is the sintering rate constant,  $L_0/\Delta L$  is the compaction rate, t is the sintering time, A is a constant related to surface tension, diffusion coefficient, and grain size, Q is the activation energy of tantalum (413.3 kJ/mol), R is the universal gas constant, and T is the temperature in Kelvin [20]. Equations 6 and 7 show that the increase in the deformation rate in the first stage of sintering

depends on the surface area, the activation energy of tantalum, and grain size. According to Equation 6, the increased surface area of tantalum powder promotes diffusion during sintering. Finer tantalum powder particles result in a larger surface area and higher surface free energy, which spontaneously decreases to a lower energy state. As sintering time increases, the density of the sample increases.

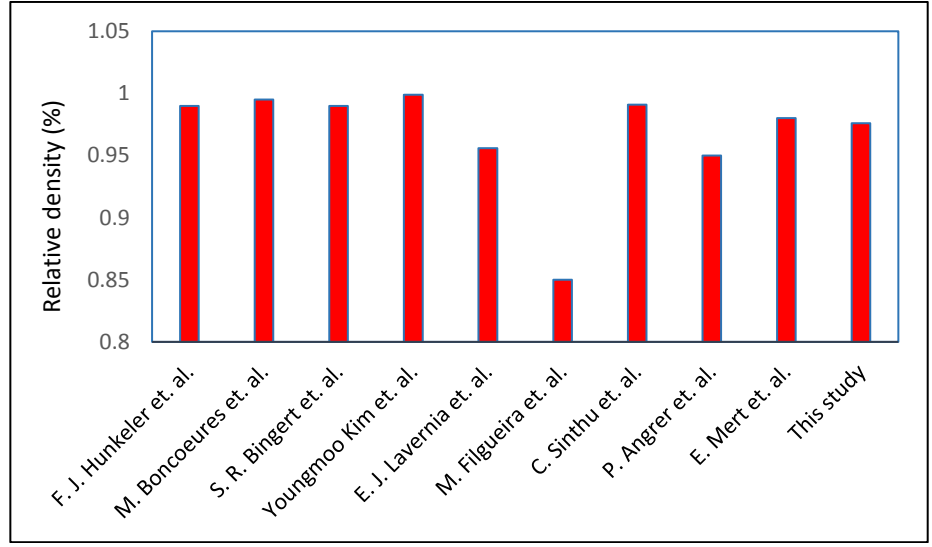


Fig. 5. Density Diagram Based on Sintering Methods.

Figure 5 presents a relative density diagram comparing various sintering methods from previous studies. The highest density in sintered tantalum samples was achieved using hot isostatic pressing (HIP). Angerer et al.'s study, which employed hot pressing at 1700°C, reported a density of 95% of the theoretical density, similar to the method used in this study. In contrast, the present study achieved a theoretical density of 97.5% at 1600°C. At 1500°C and 60 minutes, the density reached 80% of the theoretical density, while at 1500°C and 25 minutes, a density of 95.65% was attained. The higher density in this study compared to Angerer et al.'s can be attributed to increased pressing pressure. Angerer et al. used a pressure of 30 MPa, whereas this study applied 40 MPa.

Zinto's studies demonstrated that the yield strength of tantalum decreases with increasing temperature: 200 MPa at room temperature, 50 MPa at 400°C, and 34 MPa at 1000°C [18]. Therefore, it can be concluded that due to the decrease in the yield strength of tantalum at high temperatures, the increase in pressing pressure has increased the density. The increase in pressure in the sintering process leads to the rearrangement of atoms, the

breaking of particle agglomerates, and the mechanical collection of Porosity. The increase in pressure increases the sintering force. The effect of applied pressure on density can be explained using Equation (8).

$$\frac{d\rho}{(1-\rho)}dt = B\left(g\left(\frac{y}{x}\right) + P\right) \tag{8}$$

In this relation, ρ is the relative density, B is a term including diffusion coefficient and temperature, g is a geometric constant, x is a parameter related to particle size, and P is the applied external pressure [18]. According to Equation 8, it can be seen that the condensation rate increases with increasing pressure. Mort et al. reported that, during hot pressing of tantalum powder at 1500°C, a pressure of 50 MPa significantly increased density [11].

Figure 6 shows optical microscope images of the microstructure of the sintered samples. The microstructure consists of grains and porosity, with porosity observed both within grains and at grain boundaries. At 1400°C, the porosity appeared interconnected. At 1600°C, grain boundaries migrated away from the porosity, trapping it within the grains and resulting in isolated porosity.

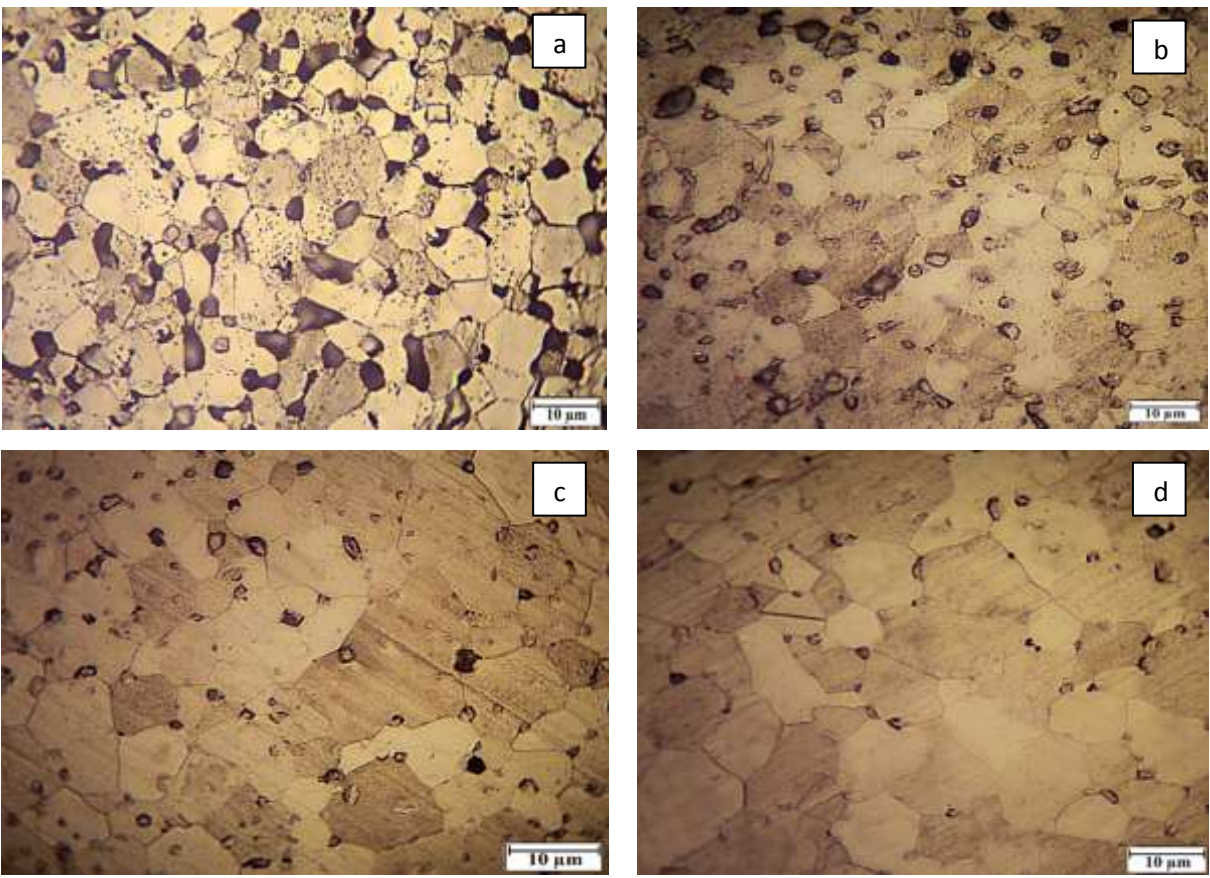


**Fig. 6.** Optical Microscope Image of Microstructure (a) Sample Sintered at 1400°C and 20 min (b) Sample Sintered at 1500°C and 15 min (c) Sintered at 1500°C and 25 min (d) Sample Sintered at 1600°C and 20 min.

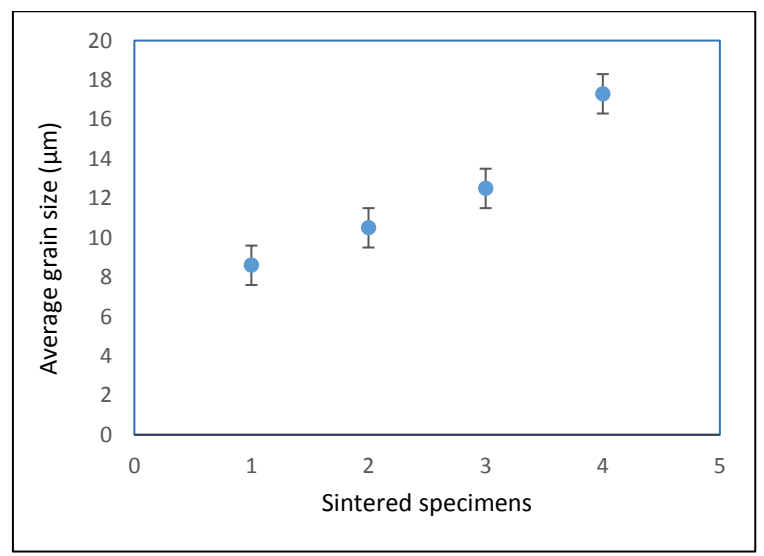


Fig. 7. Average Grain Size of Sintered Samples

Figure 7 illustrates the average grain size of the sintered samples. Microstructural analysis revealed that the grain size in tantalum increased with higher sintering temperatures. Specifically, as the temperature rose from 1400°C to 1600°C, the average grain size increased from 8.6  $\mu$ m to 17.3  $\mu$ m. Similarly, extending the sintering time from 15 to 25 minutes resulted in an increase in average grain size from 10.5  $\mu$ m to 12.5  $\mu$ m. Grain growth occurs primarily during the final stage of intermediate

sintering, where the average grain size increases while the number of grains decreases. At 1600°C, the average grain size was approximately double that observed at 1400°C.

Grain growth is driven by the reduction of grain boundary energy, as larger grains minimize the grain boundary area. Higher temperatures and longer sintering times enhance atomic diffusion along grain boundaries, facilitating grain boundary migration. Both temperature and sintering time significantly influence grain size. Limited studies have reported achieving full density in tantalum sintering with minimal grain growth.

Figure 8 compares grain sizes from this study with those from previous research. The largest grain size,

169.4 μm, was reported in Zento's study, which utilized the Field-Assisted Sintering Technique (FAST) [18]. Lavernia et al. investigated tantalum powder sintering via hot isostatic pressing (HIP), reporting a grain size of 110 μm [21].

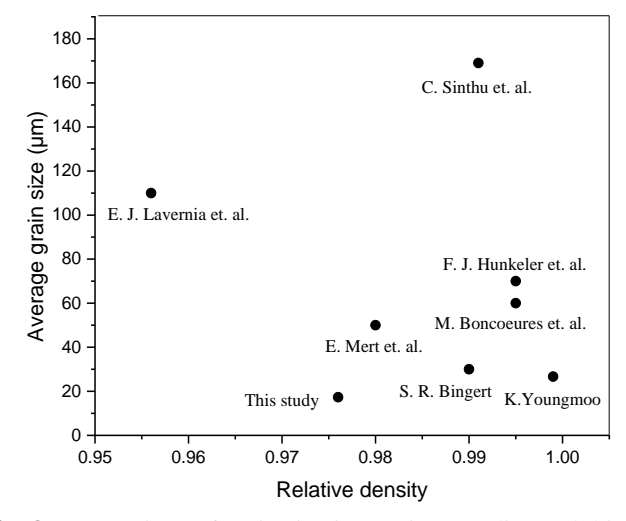


Fig. 8. Comparison of grain size in previous studies and this study.

Filgura et al. studied the effect of adding 1% nickel during pressureless liquid-phase sintering of tantalum at 2000°C for one hour, achieving a grain size of 5  $\mu$ m. However, the relative density in their study was below 85% of the theoretical density [22]. Other studies using HIP reported grain sizes of 70  $\mu$ m (Henkler), 60  $\mu$ m (Ben-Koor), and 30  $\mu$ m (Beningert) [23–25]. Grain growth was observed in all these studies.

In contrast, Yang Mo Kim et al. successfully mitigated grain growth during tantalum powder sintering by combining cold isostatic pressing with HIP [26]. Angerer et al. examined tantalum powder with a particle size of 2.4 µm using spark plasma sintering (SPS) and hot pressing (HP), achieving a

relative density of 95% in both methods. Lower sintering temperatures were found to prevent grain coarsening. In the present study, sintering at 1600°C using hot pressing in a vacuum yielded neartheoretical density with a fine-grained, homogeneous microstructure.

Temperature and sintering time also influence the morphology and extent of porosity in tantalum. Porosity is expressed as the volume percentage relative to the total volume of the sample. As stress concentration sites, pores are prone to crack initiation and propagation. The percentage and morphology of porosity significantly affect deformation behavior. Figure 9 presents the porosity percentage of the sintered samples.

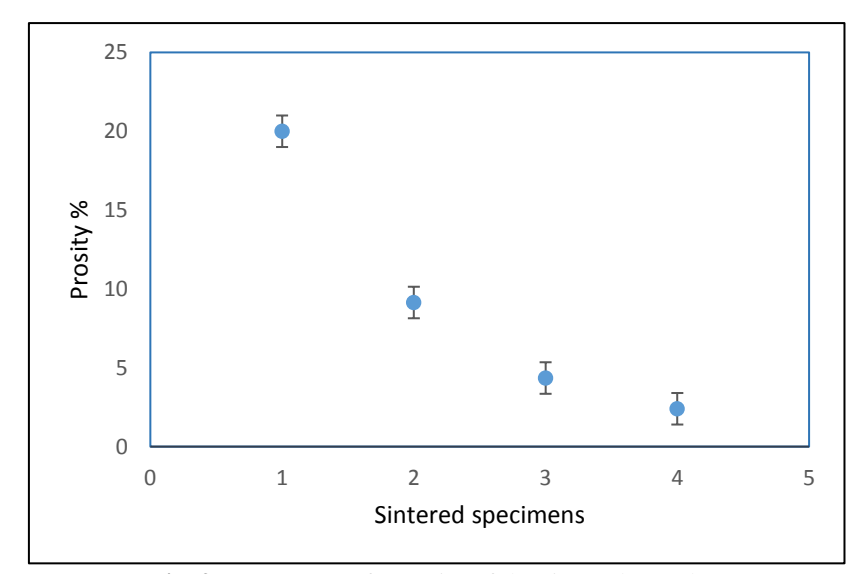


**Fig. 9.** Percentage of porosity of the sintered samples.

Figure 9 illustrates the effect of sintering temperature on porosity. As the temperature increased from 1400°C to 1600°C, the porosity percentage decreased from 20% to 2.4%, a reduction of 17.6%. Similarly, extending the sintering time from 15 to 25 minutes

reduced the porosity from 9.14% to 4.35%. The properties of powder metallurgy components are significantly influenced by the shape and distribution of porosity, which may be isolated (closed), interconnected (open), or a combination of both.

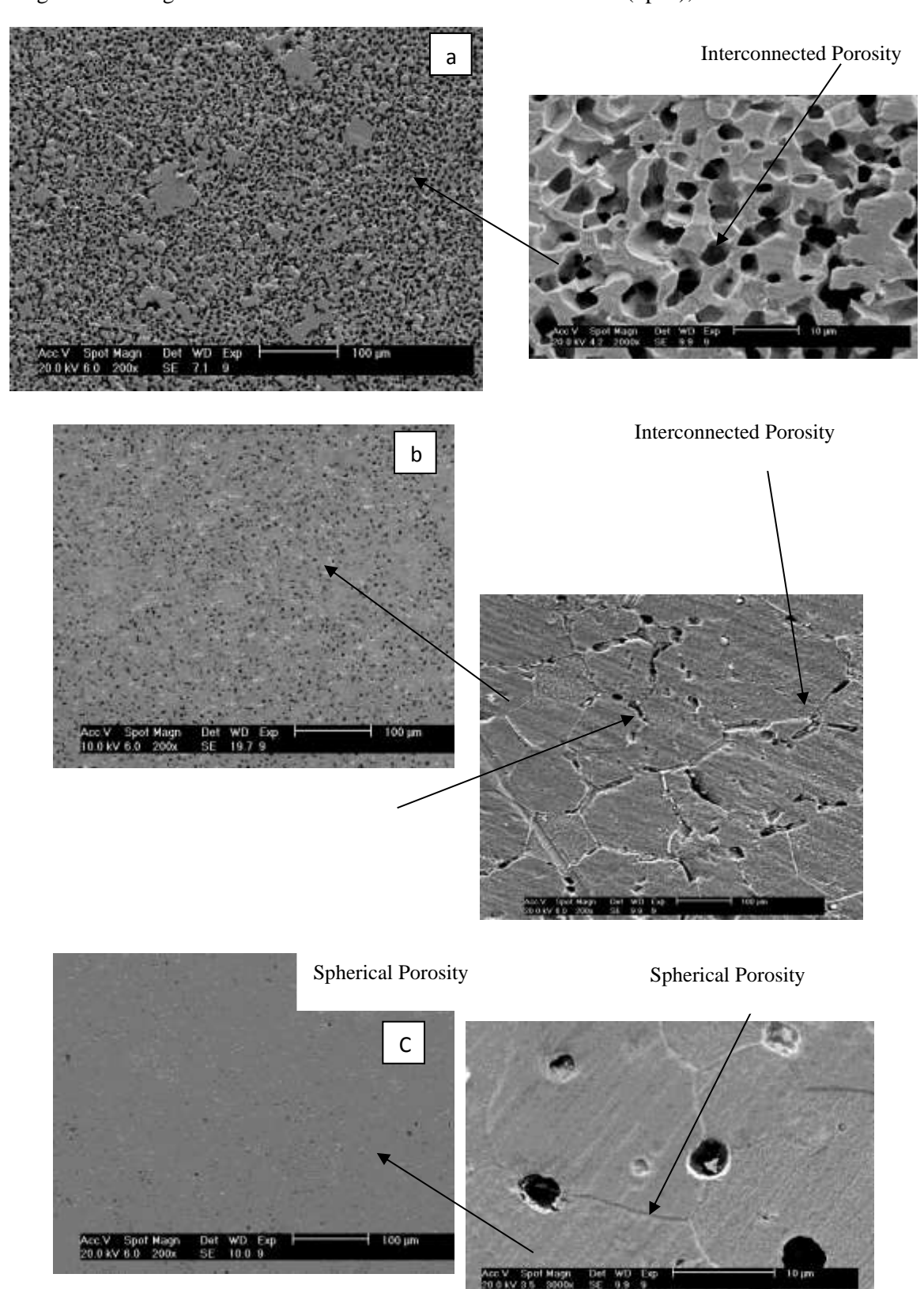


**Fig. 10.** Electron microscope image of Porosity morphology in the microstructure of (a) sample sintered at 1400°C for 20 min, (b) sample sintered at 1500°C for 25 min, and (c) sample sintered at 1600°C for 20 min.

Figure 10 presents scanning electron microscope (SEM) images of porosity morphology in the microstructure of sintered samples: (a) sintered at 1400°C for 20 minutes, (b) sintered at 1500°C for 25 minutes, and (c) sintered at 1600°C for 20 minutes. At 1400°C, the porosity was irregular and interconnected. At 1500°C, the microstructure exhibited a mix of interconnected and spherical porosity. At 1600°C, the porosity was predominantly dispersed and isolated, with a significant reduction in overall porosity. Higher sintering temperatures and longer times increased density, resulting in more uniform porosity distribution, a shift toward spherical

porosity shapes, and a decrease in interconnected porosity.

Figure 11 displays the maximum equivalent diameter (D\_circle) of porosity across four samples. At 1400°C, the D\_circle was 13.725  $\mu m$ , while at 1600°C, it decreased to 8.17  $\mu m$ , reflecting a 59.5% reduction. For samples sintered at 1500°C, increasing the sintering time from 15 to 25 minutes reduced the D\_circle from 8.919  $\mu m$  to 8.572  $\mu m$ . Porosity serves as a site for crack initiation and propagation, and larger equivalent diameters correlate with reduced mechanical properties due to increased stress concentration

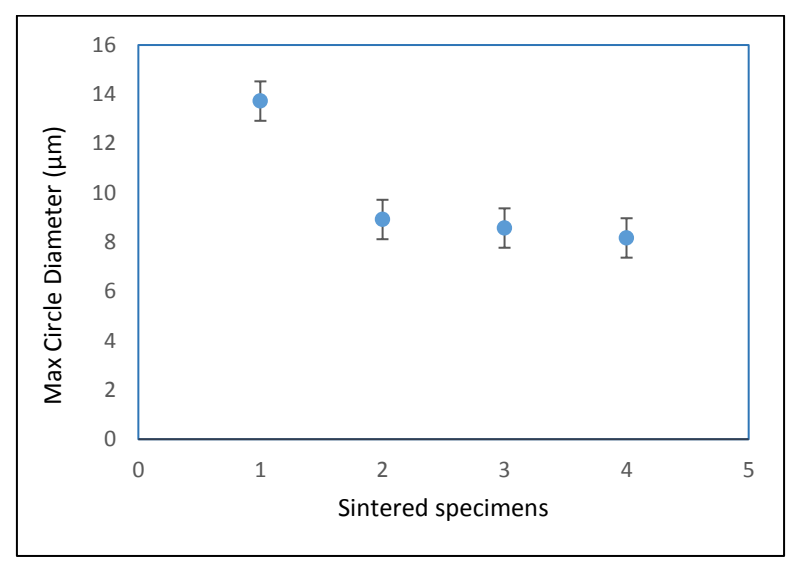


Fig. 11. Maximum equivalent diameter in sintered samples.

Figure 12 shows the Vickers hardness of the sintered samples, with the highest value of 345 HV achieved at 1600°C for 20 minutes. This value is comparable to the 341 HV reported by Engerer et al. for hot-

pressed samples at 1700°C for 60 minutes, indicating similar hardness outcomes despite differences in processing conditions.

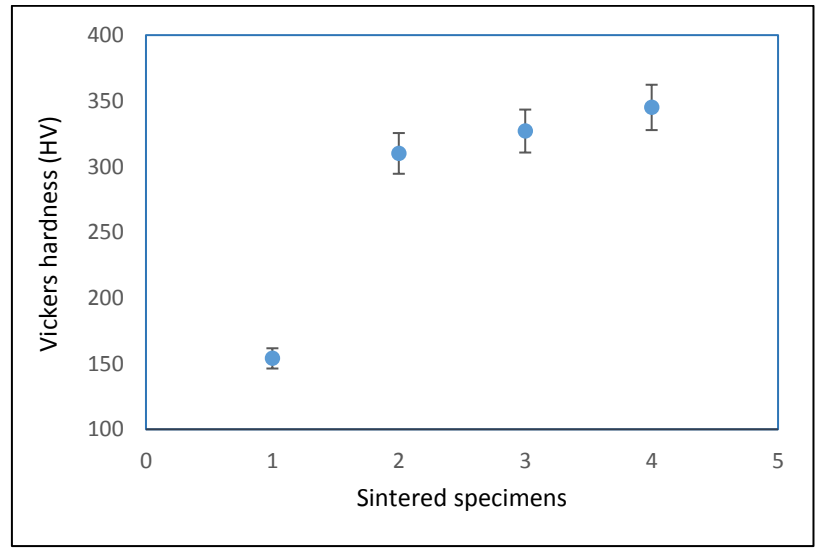


Fig. 12. Vickers hardness of sintered samples

Figure 13 shows the relationship between hardness and relative density. Hardness increased with density,

from 154 HV at 80% relative density to 310 HV at 90.8% relative density, and further to 345 HV at

97.6% relative density. This variation is attributed to improved sintering behavior, reduced porosity, changes in porosity morphology, and a decrease in the equivalent diameter of porosity. Specifically, as relative density increased from 80% to 90.8%, porosity decreased from 20% to 9.14% (a 10.86% reduction), and the D\_circle decreased from 13.725 µm to 8.919 µm (approximately 35%). With a further increase in relative density from 90.8% to 97.6%, porosity decreased from 9.14% to 2.4% (a 6.8% reduction), and the D\_circle decreased from 8.919 µm to 8.17 µm (approximately 8%). The higher rate

of porosity and D\_circle reduction at lower densities ranges explains the more significant hardness improvement in this range.

Porosity acts as a stress concentration site, promoting crack nucleation and growth, which reduces mechanical properties. The geometry and distribution of porosity significantly influence mechanical performance. Spherical and isolated porosity mitigates stress concentration compared to irregular, interconnected porosity, leading to improved mechanical properties with increased density.

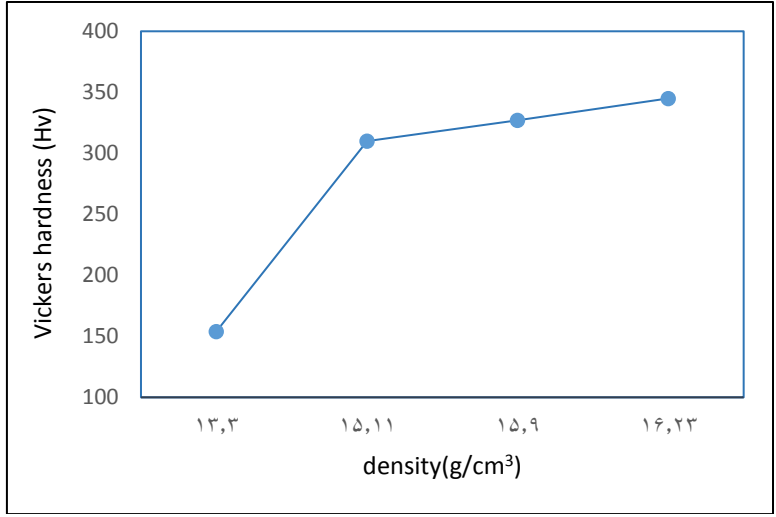


Fig. 13. Graph of hardness versus density

Figure 14 presents the true stress-strain diagram of the samples after compression testing. Figure 15 shows the compressive strength and elongation of sintered tantalum samples. As the sintering temperature increased from 1400°C to 1600°C, compressive strength rose from 327 MPa to 1278 MPa, and elongation increased from 3.6% to 34%.

Similarly, increasing the sintering time from 15 to 25 minutes enhanced compressive strength from 980 MPa to 1044 MPa and elongation from 7.8% to 18.85%. These improvements highlight the critical role of sintering temperature and time in enhancing yield strength and ductility, particularly for high-strain-rate applications.

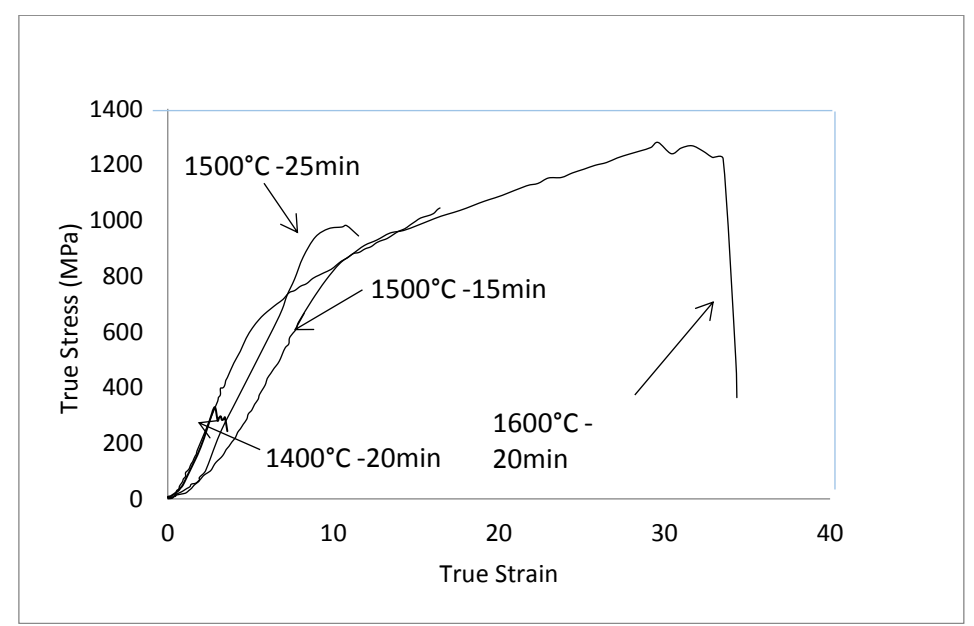


Fig. 14. True stress-strain diagram of sintered samples

1400 40 Compressive strenght (MPa) 35 1200 of elongation (%) 30 1000 25 800 20 600 15 400 10 200 5

۲

compressive strength

Fig. 15 shows the compressive strength and percentage elongation of the sintered tantalum samples.

Fig. 15. Compressive strength and percentage elongation of sintered samples

Sintered specimens

٣

□ percent of eleongation

As observed in Fig. 15, with an increase in temperature from 1400°C to 1600°C, compressive strength increased from 327 MPa to 1278 MPa, and with an increase in sintering time from 15 min to 25 min, the compressive strength increased from 980 MPa to 1044 MPa.

0

The percentage elongation also increased with an increase in temperature from 1400°C to 1600°C, from 3.6% to 34%, and with an increase in sintering time from 15 min to 25 min, from 7.8% to 18.85%. Figure 16 illustrates the relationship between mechanical properties and the effective load-bearing cross-sectional area percentage of the samples. As the sintering temperature increased from 1400°C to 1600°C, the effective load-bearing area percentage rose from 69.86% to 99.05%. Similarly, extending the sintering time from 15 to 25 minutes increased the effective load-bearing area percentage from 81.78% to 96.89%. With an increase in the effective loadbearing area from 69.86% to 81.78%, hardness increased from 150 HV to 310 HV, compressive strength rose from 327 MPa to 980 MPa, and elongation increased from 3.6% to 7.8%. Further increasing the effective load-bearing area from 81.78% to 96.89% resulted in hardness rising from 310 HV to 327 HV, compressive strength from 980 MPa to 1044 MPa, and elongation from 7.8% to 18.85%. At 99.05% effective load-bearing area, hardness reached 345 HV, compressive strength increased to 1278 MPa, and elongation rose to 34%. These results demonstrate that an increase in the effective load-bearing area significantly enhances mechanical properties.

0

۴

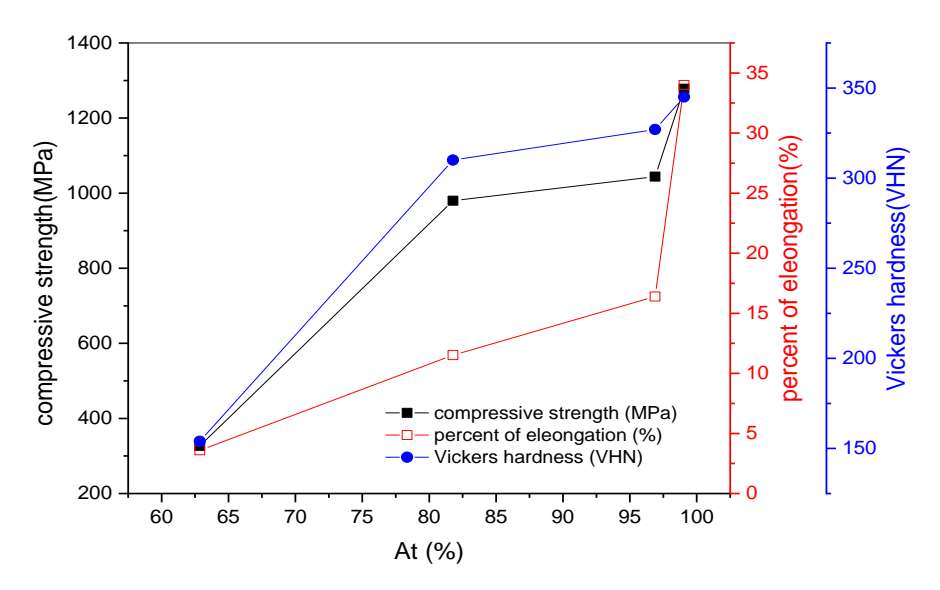


Fig. 16. Mechanical properties as a function of the effective load-bearing cross-sectional area percentage of the samples.

Figure 17 presents the mechanical properties as a function of porosity percentage. As porosity increased, hardness, compressive strength, and elongation decreased. Under uniform compressive loading, higher porosity reduces the effective loadbearing cross-sectional area, leading to stress concentration and diminished mechanical properties. Additionally, porosity morphology influences mechanical performance. Establishing a more direct relationship between microstructural changes, particularly pore morphology, mechanisms in compression testing can provide a better understanding of the material's mechanical behavior. As shown in Figure 10 (SEM images), interconnected and irregular porosity at 1400°C acts as stress concentration sites, promoting crack initiation and propagation. In contrast, at 1600°C, isolated and spherical porosity results in more uniform stress distribution, delaying crack initiation and enhancing ductility (evidenced by an increase in elongation from 3.6% at 1400°C to 34% at 1600°C and compressive strength (from 327 MPa to 1278 MPa). Interconnected porosity at lower temperatures facilitates crack propagation, while spherical porosity at higher temperatures improves resistance to crack growth. Spherical porosity promotes uniform deformation before fracture, whereas irregular porosity with sharp edges creates stress concentration regions, reducing elongation. Microstructures with interconnected porosity exhibit a greater reduction in mechanical properties compared to those with isolated porosity.

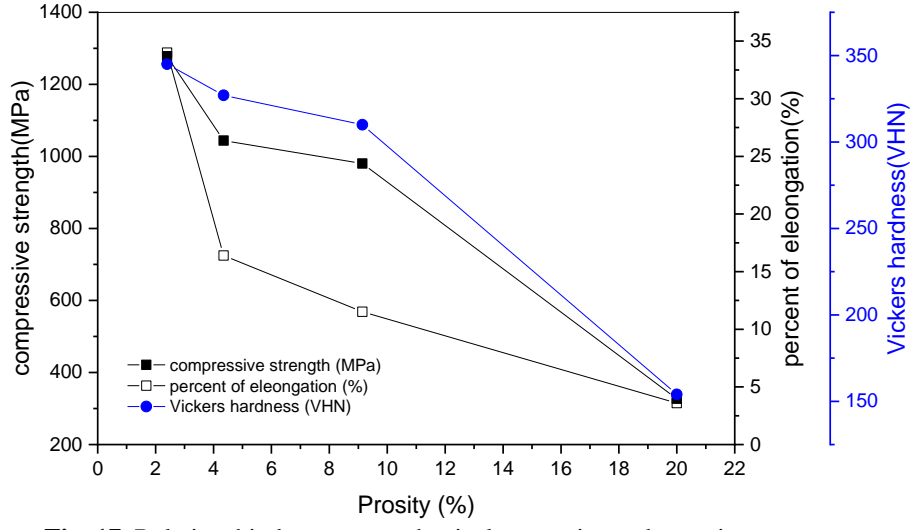


Fig. 17. Relationship between mechanical properties and porosity percentage.

The study also revealed that increasing relative density from 80% to 97.6% (a 17.6% increase) improved hardness from 150 HV to 345 HV, compressive strength from 327 MPa to 1278 MPa, and elongation from 3.6% to 34%, representing a 100% increase in these properties. This underscores the critical role of density in enhancing mechanical performance. Higher density increases Young's modulus, improving the material's ability to withstand stress before fracture. Furthermore, as density increased, porosity distribution became more uniform, as evidenced by the porosity morphology analysis.

Figure 18 depicts the mechanical properties as a function of average grain size. As the sintering temperature increased from 1400°C to 1600°C, the average grain size grew from 8.6  $\mu$ m to 17.3  $\mu$ m, with hardness increasing from 150 HV to 345 HV, compressive strength from 327 MPa to 1278 MPa, and elongation from 3.6% to 34%. Similarly, increasing the sintering time from 15 to 25 minutes resulted in grain size growth from 10.5  $\mu$ m to 12.5  $\mu$ m, with hardness rising from 310 HV to 327 HV,

compressive strength from 980 MPa to 1044 MPa, and elongation from 7.8% to 18.85%. According to the Hall-Petch relationship, an increase in grain size is typically associated with a decrease in strength and hardness, as grain boundaries act as barriers to dislocation movement. However, in the present study, an improvement in mechanical properties (such as hardness, compressive strength, and elongation) was observed despite the increase in grain size, primarily due to the dominant effects of reduced porosity and increased relative density. As the temperature increased from 1400°C to 1600°C, the relative density rose from 80% to 97.6%, and the porosity decreased from 20% to 2.4%. This significant reduction in porosity increased the effective load-bearing cross-sectional area (from 69.86% to 99.05%), which had a stronger positive impact on mechanical properties compared to the negative effect of grain growth (from 8.6 micrometers to 17.3 micrometers). Despite the increase in grain size with higher temperature and sintering time, mechanical properties improved, highlighting the dominant influence of density and

porosity reduction over grain size effects. Using Equation 8, it can be shown that increased pressure and temperature led to higher densification and reduced porosity, directly increasing the effective

cross-sectional area and improving mechanical properties. In the study by Mort et al., an increase in pressing pressure also resulted in improved density and mechanical properties.

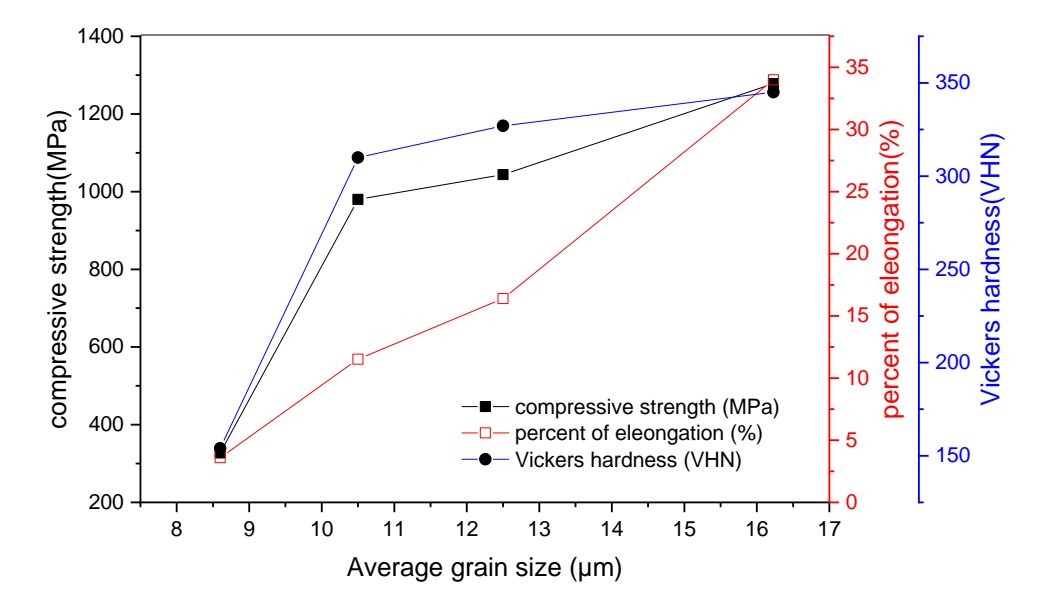


Fig. 18. Graph of mechanical properties as a function of average grain size.

The enhancement of mechanical properties in sintered tantalum components can be attributed to the influence of microstructure and porosity morphology. In parts with low porosity, the microstructure predominantly governs mechanical performance, whereas in high-porosity parts, porosity morphology is the primary factor. In lowdensity porous components, porosity controls crack propagation, with the microstructure playing a minimal role. Conversely, in high-density components, the microstructure is the dominant factor in crack growth.

This study examined the impact of powder metallurgy process parameters, specifically sintering temperature and time, on the microstructure and mechanical properties of hot-pressed sintered tantalum. The findings indicate that increasing density, reducing porosity, expanding the effective load-bearing area, and modifying porosity morphology enhance the ductility and mechanical properties of sintered tantalum, despite an increase in average grain size.

#### 4. Conclusions

This study demonstrates that hot pressing (HP) consolidation of pure tantalum powder significantly enhances its mechanical properties by reducing porosity and modifying porosity morphology. A 17.6% increase in density resulted in a remarkable 100% improvement in compressive strength, ductility, and hardness. Optimal mechanical properties were achieved at a sintering temperature of

1600°C, yielding a hardness of 345 HV, compressive strength of 1278 MPa, and ductility of 34%. These findings underscore the critical role of optimizing sintering temperature and time to achieve superior mechanical performance in tantalum, offering valuable insights for advanced material processing applications.

#### 5. Novelty and Contribution

This study provides novel insights into the optimization of hot pressing (HP) parameters for consolidating pure tantalum powder, addressing critical gaps in the existing literature on tantalum's sintering behavior. By systematically investigating the effects of sintering temperature and time on microstructure and mechanical properties, this work establishes a direct correlation between reduced porosity, modified porosity morphology, and significant enhancements in mechanical performance. The achievement of a 17.6% increase in density, resulting in a 100% improvement in compressive strength (1278 MPa), ductility (34%), and hardness (345 HV) at an optimal sintering temperature of 1600°C, represents a substantial advancement in the processing of tantalum.

# **6. Conflict of Interest**

All authors declare no conflict of interest.

# 7. Funding

The authors did not receive funding to conduct the research.

#### References

- [1] Lambert, J.B, "Properties and Selection: Nonferrous Alloys and Special-Purpose Materials", ASM Handbook, Vol. 2, (1990), 1698-1701.
- [2] Cardonne SM, Kumar P, Muchaluk CA, Schwartz HD, "Tantalum and its alloys", Int J Refract Met Hard Mater, 13, (1995), 187–94.
- [3] Lambert, J.B, "Properties and Selection: Nonferrous Alloys and Special-Purpose Materials", ASM Handbook, Vol. 2, (1990), 557-585.
- [4] Buckman Jr RW, "New Applications for Tantalum and Tantalum Alloys", J Miner Met Mat Society, 52, 3, (2000), 40-41.
- [5] Burns RH, Fang JC, Kumar P, "Evolution of applications of tantalum", Proc 125th TMS AnnualMeeting and Exhibition, (1996), 273–85.
- [6] Chou, PC, Crudza, ME, "The effects of liner anisotropy on warhead performance", Warrendale PA TMS, (1992), 97–109.
- [7] Muller JF, Dinh, PM, "Evaluation of powder metallurgy tantalum liners for explosively formed penetrator", Proc 2nd Int Conf Tungsten Refract Met,(1994), 573–86.
- [8] Flater P, House J, O'Brien J, HosfordWF, "High strain rate properties of tantalum processed by equal channel angular pressing", Air Force Research Laboratory Technical Report, (2007), 7412.
- [9] W. Brian James, Hoeganaes Corporation, retired, "Powder Metallurgy Methods and Application", ASM Handbook, Vol. 07, (2015), 1424-1445.
- [10] Yoo SH, Sudarshan TS, Sethuram K, Subhash G, Dowding RJ, "Consolidation and high strain rate mechanical behavior of nanocrystalline tantalum powder", Nanostruct Mater, 12, (1999), 23–8.
- [11] Mert Efe, Hyun Jun Kim, Srinivasan Chandrasekar, Kevin P. Trumble, "The chemical state and control of oxygen in powder metallurgy tantalum", Materials Science and Engineering, A, 544, (2012), 1–9.
- [12] Stecura, S, Metall. Trans, 5, (1974), 1337–1340.
- [13] Droegkamp R.E, Schussler M, Lambert J.B, Taylor D.F, Encyclopedia of Chemical Technology, vol. 22, (1984), 541–564.
- [14] Mann J.B, Saldana C, Chandrasekar S, Compton W.D, Trumble K.P, Scr. Mater, 57, (2007), 909–912.

- [15] Angerer P, Neubauer E, Yu LG, Khor KA, "Texture and structure evolution of tantalum powder samples during spark-plasma-sintering and conventional hot-pressing", Int J Refract Met Hard Mater, 25, (2007), 280–5.
- [16] Angerer P, Artner W, Neubauer E, Yu LG, Khor KA, "Residual stress in spark-plasma-sintered and hot-pressed tantalum samples determined by X-ray diffraction methods", International Journal of Refractory Metals & Hard Materials, 26, (2008), 312–317.
- [17] Khorsand, H.; Abdoos, H. (2015). Mechanical and Fatigue Behavior of Sintered Porous Parts. Tehran: University of Khajeh Nasirodin Toosi. (In Persian)
- [18] Sinthu Chanthapan, "sintering of refractory metal based materials by firld assisted sintering technology (FAST) ",Doctoral dissertation in material science, Pennsylvania State University,(2012).
- [19] Brown AM, Ashby MF, "Correlations for Diffusion Constants", Journal of Acta Metallurgica, (1980), 1085.
- [20] German R M, "Sintering Theory and Practice". New York: John Wiley and Sons, (1996).
- [21] Xu Q, Hayes RW, Lavernia EJ. "Creep properties of ball-milled and HIPed pure tantalum". Scr Mater (2001),45, 447–54.
- [22] Filgueira M, Pinatti DG, De Holanda JNF, Gomes UU. "Densification and mechanical properties of liquid phase sintered tantalum". Mat-wiss, u Werkstofftech, (2009), 40, 784-790.
- [23] Funkeler FJ, "Fabricated tantalum from unsintered HIP powder", Tungsten and refractory metals, Proc 2nd Int Conf Tungsten Refract Met, MPIF: McLean; October (1994), 531–46.
- [24] Boncoeur M, Valin F, Raisson G, Michaud H. "Properties of hot isostatically pressed tantalum. Hot isostatic pressing-theory and applications", Proc 3rd Int Conf Hot Isostatic Pressing, Osaka, Springer, (1991), 247–52.
- [25] Bingert SR, Vargas VD, Sheinberg H, "Tantalum powder consolidation, modeling and properties Tantalum", Proc 125th TMS Annual Meeting and Exhibition, Anaheim TMS, (1996), 95–105.
- [26] Youngmoo Kim, "Fabrication and mechanical properties of powder metallurgy tantalum prepared by hot isostatic pressing", Int. Journal of Refractory Metals and Hard Materials, (2015),48, 211–216.